



ORIGINAL ARTICLE

Non-soluble chalcones and their potential application as corrosion coatings on carbon steel exposed to 1 M HCl solutions



Carlos Andrés Coy-Barrera*, Inti Camilo Monge, Diego Quiroga

Bioorganic Chemistry Laboratory, Facultad de Ciencias Básicas y Aplicadas, Campus Nueva Granada, Universidad Militar, Nueva Granada, Cajicá 250247, Colombia

Received 8 July 2022; accepted 21 November 2022

Available online 25 November 2022

KEYWORDS

Claisen-Schmidt reaction;
Chalcone derivatives;
Impedance;
Potentiodynamic polarization;
Coating

Abstract Chalcones are secondary metabolites of great interest in chemistry due to their broad biological activities. In recent years, the versatility of this class of molecules has been demonstrated, especially in several synthetic analogs, which have shown behavior as corrosion inhibitors. In this article, a series of chalcone analogs were synthesized using the Claisen-Schmidt methodology in both conventional and microwave-assisted irradiation methodologies. The obtained compounds are non-soluble, which widens the window of chalcones with the possibility of being used as anti-corrosive. These were analyzed by electrochemical impedance spectroscopy, potentiodynamic polarization, weight loss measurements and scanning electron microscopy. The results suggest that the chalcone compounds such as the trans-4-(N,N-diphenylamino)chalcone (CH11), (E)-1-phenyl-3-(thiophen-2-yl)prop-2-en-1-one (CH15) and (E)-1-phenyl-3-(thiophen-3-yl)prop-2-en-1-one (CH16) have anticorrosive activity for carbon steel in HCl solutions. The electrochemical techniques showed that increasing the mass of the three chalcone on carbon steel increases the efficiency of the inhibition. A mass amount of 1.4 mg of CH15 or CH16 was shown to have the maximum inhibition from corrosion, but for CH11 the maximum inhibition was 3.0 mg on carbon steel. The percentage inhibition that reached these three compounds was about 95 % at 20 °C. Theoretical calculations by Density Functional Theory (DFT) were performed to explain the measured corrosion decrease assisted by compounds CH11, CH15, and CH16.

© 2022 The Author(s). Published by Elsevier B.V. on behalf of King Saud University. This is an open access article under the CC BY-NC-ND license (<http://creativecommons.org/licenses/by-nc-nd/4.0/>).

* Corresponding author.

E-mail address: carlos.coy@unimilitar.edu.co (C. Andrés Coy-Barrera).

Peer review under responsibility of King Saud University.



1. Introduction

Chalcone compounds are a group of molecules with a great interest in Chemistry. Their different analogs and derivatives have been widely studied for their known biological activity (Sahu et al., 2012). Their use as ligand to afford ferrocenyl-Cimanthrenyl chalcone bimetallic complexes is broadly known. These compounds have shown potential anti-malarial, anti-cancer, anti-microbial, and anti-inflammatory properties (Mishra et al., 2015). In addition to the above, chalcone analogs have mainly been used due to their ease of synthesis, which possesses advantages such as high efficiency, uncomplicated work-up procedure, and scalability. Recently, several applications have been developed, such as their use as a precursor of fluorescent supramolecular columnar liquid crystals derived from chalcone and biphenylamine. These materials have shown interesting photophysical and electrochemical properties, such as emission of blue light in solution and thin films, with good quantum yields, later used to manufacture organic light-emitting diodes (OLED) (Sharma et al., 2020).

Furthermore, a vinylene-phenylene oligomer was electro-synthesized by the oxidation of 4-dimethylamino-4'-methoxychalcone (DMAMC), showing promising application for the design of new materials thermally stable and with absorption capacities in the yellow-orange zone (Messaoudi et al., 2021). Moreover, five derivatives of chalcones (Abegão et al., 2020) showed that a minor molecular structure modification could trigger a significant optical response to be used as potential raw materials to build ultrafast optical switches or optical limiting devices. These results demonstrated that the size of the molecule is an essential parameter to improve this characteristic previously mentioned, even if molecules with a short length could also achieve good optical responses. The synthesis, characterization, and applications of functional polymers derived from thiophene have been extensively studied. Several reports related to polyphenols are included in literature reviews on conductive polymers, electrochemistry, stability, or optical properties in electropolymerization articles (Blasco et al., 2004; Bouklah et al., 2006; Doménech-Carbó et al., 2018; Martínez-Cifuentes et al., 2015; Pérez-Cruz et al., 2013; Serifi et al., 2013; Shah et al., 2010; Slobodinyuk et al., 2020; Tavares et al., 2013). The applications of conductive polymers are numerous and varied, including organic batteries, electrochromic viewers, chemical sensors, light-emitting diodes (LEDs), radar blockers, anti-corrosion additives, and water purification membranes. However, its most spectacular applications are undoubtedly in biomedicine and biotechnology. In this context, the design of analytical devices with interactions specific: artificial muscles and nerves, sensors for the recognition of biomolecules, and drug-releasing systems (Doménech-Carbó et al., 2018).

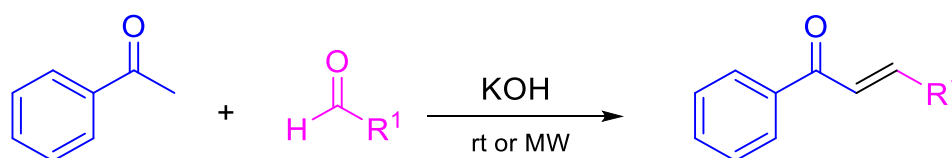
The use of potentiodynamic measurements of resistance to polarization and weight loss, resistance to linear polarization (LPR), electrochemical impedance spectroscopy (EIS), and electrochemical frequency modulation (EFM) has shown that the addition of chalcones -such as naphthylchalcone derivatives, 4'-dihydroxychalcone, (*E*)-3-(4-hydroxyphenyl)-*N*-phenylacrylamide, (*E*)-3-(4-dimethylamino)phenyl)-*N*-phenylacrylamide and (*E*)-3-(4-hydroxy-3-methoxyphenyl)-*N*-phenylacrylamide- could reduce corrosion rate by increases the concentration of these species. The addition of chalcones increases the charge transfer resistance and decreases the double-layer capacitance of the corrosion process. In addition, it was shown that this type of compound acts as a cathodic inhibitor and is adsorbed on the surface

of steel according to the Langmuir adsorption isotherm model (A.S. Fouda, K. Shalabi, G.Y. Elewady, 2014; A.S. Fouda, A.F. Hassan, M. A. Elmorsi, T.A. Fayed, 2014; Chaouiki et al., 2020; Fouda, A. S., Gadaw, H. S., El-Shafei, 2003; Lgaz et al., 2017; Pooja Singh, M.A. Quraishi, E.E. Ebenso, 2014; Ramaganthan et al., 2015; Velrani, S., Mahalakshmi, 2015). Studies of potentiostatic polarization and resistance to polarization have shown that some chalcones act as effective inhibitors of nickel corrosion in 1 M HCl and 0.5 M H₂SO₄, predominantly cathodic inhibitors in both acids (Kumar et al., 2020). Studies using some chalcone derivatives like (*E*)-3-(4-methoxyphenyl)-1-(*p*-tolyl)prop-2-en-1-one evidenced that the adsorption of chalcones on the surface of the metal decrease the corrosion of mild steel samples. This result was confirmed by SEM and AFM studies and compared with non-inhibited models. The inhibition of mild steel corrosion has been also demonstrated in 0.5 M H₂SO₄ using ethanolic extracts of *Chromolaena odorata L* using a gravimetric technique in the temperature range 30–60 °C. This result was associated with the presence of essential oils, steroids, triterpenes, as well as the high content of a series of complex flavonoids, chalcones, and flavones in the extract (I.B. Obot, E.E. Ebenso, 2021; Olasehinde et al., 2022). A series of mild steel chalcone-based corrosion inhibitors was recently synthesized using azoacetophenone and substituted aromatic aldehydes (Assad and Kumar, 2021). The corrosion inhibitory activity of the synthesized chalcones was studied by the acidimetric and weight loss method for mild steel in 1 M hydrochloric acid. The experimental results showed that the inhibition efficiency of all corrosion inhibitors increases with an increase in concentration and decreases with increasing temperature. The good inhibition activity is attributed to forming a protective layer on mild steel surfaces described previously (Katharotiya P., 2021). Considering these antecedents, and the structural variation of the chalcones the present research seeks to study the possible inhibitory effect of corrosion by chalcones of low solubility in the water once deposited on the surface of carbon steel in 1.0 M HCl using electrochemical techniques such as EIS and PDP and by weight loss.

2. Experimental procedures

2.1. Materials, electrolytes, and inhibitors

The entire reagents and chemicals were commercially acquired (Merck KGaA and/or Sigma-Aldrich). They were employed without additional refinement. As a result, the purity of dry solvents was sufficiently defined during purchasing. The products' progression of reactions and purifications were monitored by thin-layer chromatography (TLC) on silica gel 60 F254 plates (Merck KGaA) under detection at 254 nm. Microwave-assisted reactions were performed in a CEM Discover Labmate reactor of 300 W as maximum irradiation power. Silica gel 60 (0.040–0.063 mm mesh) (Merck KGaA) was used for CC. For nuclear magnetic resonance (NMR) experiments, a Bruker Avance AV-400 MHz spectrometer was employed. TMS was utilized as a reference to give chemical shifts in δ (ppm). Typical splitting patterns were implemented to define the signal multiplicity (i.e., s, singlet; d, doublet; t, triplet; m, multiplet).



Scheme 1 Synthesis of chalcones CHI-CH16.

2.2. Chalcones derivatives synthesis

For the synthesis of chalcone-type compounds under study, Claisen-Schmidt reaction conditions were used (Yadav and Wagh, 2020), according to the following procedures (See scheme 1).

2.2.1. Method A: Room temperature reactions

A mixture of potassium hydroxide (KOH) (0.1 mmol), water (5 mL), ethanol (5 mL), acetophenone (1 mmol), and the aldehyde of interest (1–16, 1 mmol) was prepared in a round-bottom ball. First, the mixture was kept under constant stirring at room temperature for 8 h. Then, the reaction mixture was kept under refrigeration (0–4° C) for 12 h, during which the formation of a precipitate was observed. Next, the reaction mixture was filtered, and the solid was washed with cold water (5x10 mL). Next, the compound was dried in an oven at 50° C, and finally, it was purified by recrystallization from ethanol, affording the desired product.

2.2.2. Method B: Solvent-free microwave-assisted reactions

In a 10 mL microwave vessel were mixed potassium hydroxide (KOH) (10 % mol), acetophenone (1 mmol), and the aldehyde of interest (1–16, 1 mmol). The mixture was heated between 80 and 120 °C for 10 min under microwave radiation in a closed atmosphere. The reaction crude was neutralized using saturated ammonium chloride solution until pH 8.0, and then it was extracted using ethyl acetate (5x10 mL). The organic extract was treated with anhydrous sodium sulfate. The reaction crude was adsorbed on silica gel and then purified by column chromatography (Petroleum ether (PE) / Ethyl acetate (AcOEt) 7:3) to give the desired product. The characterization data of the obtained products are presented below:

Trans-chalcone (CH1): Yellow solid, with a melting point between 51 and 54 °C, 75 % yield. Soluble in chloroform, ethyl acetate, 1,4-dioxane. Insoluble in petroleum ether and water; ¹H NMR spectrum (400 MHz, CDCl₃) in ppm: 8.00 (m, 2H), 7.78 (d, 1H, *J* = 15.7 Hz), 7.52 (d, 1H, *J* = 15.7 Hz), 7.65–7.37 (m, 6H); ¹³C NMR spectrum (100 MHz, CDCl₃) in ppm: 190.4, 144.8, 138.2, 134.9, 132.8, 130.5, 128.9, 128.6, 128.5, 128.4, 122.1.

Trans-4-chlorochalcone (CH2): Yellow-greenish solid, with a melting point between 112 and 115 °C with decomposition, 83 % yield. Soluble in chloroform, ethyl acetate, 1,4-dioxane. Insoluble in petroleum ether and water; ¹H NMR spectrum (400 MHz, CDCl₃) in ppm: 8.00 (d, 2H), 7.73 (d, 1H, *J* = 15.8 Hz), 7.62–7.47 (m, 5H), 7.52 (d, 1H, *J* = 15.7 Hz), 7.39 (d, 2H); ¹³C NMR spectrum (100 MHz, CDCl₃) in ppm: 190.1, 143.2, 138.0, 136.4, 133.4, 132.9, 129.6, 129.2, 128.6, 128.5, 122.5.

Trans-4-(N,N-dimethylamino)chalcone (CH3): Reddish solid, with a melting point between 135 and 160 °C with decomposition, 34 % yield. Soluble in chloroform, ethyl acetate, 1,4-dioxane. Insoluble in petroleum ether and water; ¹H NMR spectrum (400 MHz, CDCl₃) in ppm: 7.73 (d, 2H, *J* = 7.5 Hz), 7.52 (d, 1H, *J* = 15.5 Hz), 7.35–7.20 (m, 3H), 7.21 (d, 1H, *J* = 7.4 Hz), 7.06 (d, 1H, *J* = 15.5 Hz), 6.41 (d, 1H, *J* = 8.1 Hz), 2.76 (s, 6H); ¹³C NMR spectrum (100 MHz, CDCl₃) in ppm: 199.0, 190.7, 152.0, 145.9, 139.1, 133.0, 130.4, 128.6, 128.3, 122.6, 111.8, 40.1.

Trans-4-hydroxychalcone (CH4): Orange solid, with a melting point between 110 and 134 °C with decomposition, 27 % yield. Soluble in chloroform, ethyl acetate, 1,4-dioxane. Insoluble in petroleum ether and water; ¹H NMR spectrum (400 MHz, CDCl₃) in ppm: 9.83 (s, 1H), 8.01 (d, 2H, *J* = 7.6 Hz), 7.79 (d, 1H, *J* = 15.5 Hz), 7.85–7.75 (m, 2H), 7.60–7.40 (m, 3H), 7.41 (d, 1H, *J* = 15.5 Hz), 6.99 (d, 2H, *J* = 8.1 Hz); ¹³C NMR spectrum (100 MHz, CDCl₃) in ppm: 191.1, 163.0, 158.4, 145.2, 138.6, 132.9, 130.7, 128.8, 128.6, 119.9, 116.2.

Trans-4-aminochalcone (CH5): Orange, resinous solid, 35 % yield. Soluble in chloroform, ethyl acetate, 1,4-dioxane. Insoluble in petroleum ether and water; ¹H NMR spectrum (400 MHz, CDCl₃) in ppm: 8.47 (d, 1H, *J* = 8.9 Hz), 8.33 (d, 1H, *J* = 15.2 Hz), 8.00–7.85 (m, 2H), 7.80–7.60 (m, 2H), 7.24–7.00 (m, 2H), 7.17 (d, 1H, *J* = 15.2 Hz), 6.73 (d, 2H, *J* = 7.3 Hz); ¹³C NMR spectrum (100 MHz, CDCl₃) in ppm: 191.1, 163.0, 158.3, 145.2, 138.5, 132.8, 130.7, 128.8, 127.8, 119.9, 116.2.

Trans-2-aminochalcone (CH6): Orange, resinous solid, 33 % yield. Soluble in chloroform, ethyl acetate, 1,4-dioxane. Insoluble in petroleum ether and water; ¹H NMR spectrum (400 MHz, CDCl₃) in ppm: 8.22 (m, 3H), 8.18 (d, 1H, *J* = 11.7 Hz), 7.86 (d, 1H, *J* = 8.6 Hz), 7.82 (d, 1H, *J* = 8.1 Hz), 7.75 (t, 1H, *J* = 7.7 Hz), 7.56 (d, 1H, *J* = 8.1 Hz), 7.54 (d, 1H, *J* = 7.7 Hz), 7.52 (d, 1H, *J* = 11.7 Hz), 7.50–7.45 (m, 1H); ¹³C NMR spectrum (100 MHz, CDCl₃) in ppm: 157.4, 148.4, 139.8, 136.8, 129.7, 129.4, 129.3, 128.9, 127.7, 127.5, 127.4, 126.3, 119.1.

Trans-4-nitrochalcone (CH7): Yellow, resinous solid, 75 % yield. Soluble in chloroform, ethyl acetate, 1,4-dioxane. Insoluble in petroleum ether and water; ¹H NMR spectrum (400 MHz, CDCl₃) in ppm: 8.30 (m, 2H), 8.07 (m, 2H), 7.85–7.76 (m, 3H), 7.75–7.60 (m, 2H), 7.58–7.50 (m, 2H); ¹³C NMR spectrum (100 MHz, CDCl₃) in ppm: 191.1, 147.7, 141.3, 136.5, 129.2, 129.1, 129.0, 128.9, 128.8, 125.9, 124.4.

Trans-4-methoxychalcone (CH8): Yellow, resinous solid, 38 % yield. Soluble in chloroform, ethyl acetate, 1,4-dioxane. Insoluble in petroleum ether and water; ¹H NMR spectrum (400 MHz, CDCl₃) in ppm: 8.07 (d, 2H), 7.76 (d, 1H), 7.61–7.50 (m, 3H), 7.49–7.40 (m, 3H), 6.91 (d, 2H), 3.80 (s, 3H); ¹³C NMR spectrum (100 MHz, CDCl₃) in ppm: 191.1, 161.7, 144.6, 138.5, 132.6, 130.2, 128.6, 128.4, 127.6, 119.7, 114.4, 55.35.

Trans-4-bromochoalcone (CH9): Yellow, resinous solid, 69 % yield. Soluble in chloroform, ethyl acetate, 1,4-dioxane. Insoluble in petroleum ether and water; ¹H NMR spectrum (400 MHz, CDCl₃) in ppm: 8.00 (d, 2H, *J* = 7.9 Hz), 7.71 (d, 1H, *J* = 15.7 Hz), 7.60–7.40 (m, 7H), 7.54 (d, 1H, *J* = 15.7 Hz); ¹³C NMR spectrum (100 MHz, CDCl₃) in ppm: 190.2, 143.3, 138.0, 133.8, 132.9, 132.2, 129.8, 128.6, 128.5, 124.8, 122.6.

Trans-4-benzoyloxychalcone (CH10): Yellow, resinous solid, 41 % yield. Soluble in chloroform, ethyl acetate, 1,4-dioxane. Insoluble in petroleum ether and water; ¹H NMR spectrum (400 MHz, CDCl₃) in ppm: 7.99 (d, 2H, *J* = 7.7 Hz), 7.77 (d, 1H, *J* = 15.6 Hz), 7.55 (d, 1H, *J* = 8.2 Hz), 7.55–7.50 (m, 1H), 7.50–7.25 (m, 8H), 7.39 (d, 1H, *J* = 15.5 Hz), 6.97 (d, 2H, *J* = 8.2 Hz), 5.05 (s, 2H);

¹³C NMR spectrum (100 MHz, CDCl₃) in ppm: 190.4, 160.9, 144.6, 138.5, 136.4, 132.6, 130.3, 128.7, 128.6, 128.4, 128.2, 127.9, 127.5, 119.9, 115.3, 70.1.

Trans-4-(N,N-diphenylamino)chalcone (CH11): Yellow, resinous solid, 32 % yield. Soluble in chloroform, ethyl acetate, 1,4-dioxane. Insoluble in petroleum ether and water; ¹H NMR spectrum (400 MHz, CDCl₃) in ppm: 7.99 (d, 2H, *J* = 7.4 Hz), 7.77 (d, 1H, *J* = 15.6 Hz), 7.55–7.30 (m, 7H), 7.29–7.21 (m, 3H), 7.18–7.02 (m, 6H), 7.05 (d, 1H, *J* = 15.6 Hz), 7.00 (d, 2H, *J* = 8.4 Hz); ¹³C NMR spectrum (100 MHz, CDCl₃) in ppm: 190.4, 150.1, 146.8, 144.6, 138.6, 132.4, 129.8, 129.5, 128.5, 128.4, 127.8, 125.4, 124.1, 121.6, 119.4.

Trans-4-t-butoxychalcone (CH12): Yellow, resinous solid, 31 % yield. Soluble in chloroform, ethyl acetate, 1,4-dioxane. Insoluble in petroleum ether and water; ¹H NMR spectrum (400 MHz, CDCl₃) in ppm: 8.01 (d, 2H, *J* = 7.8 Hz), 7.79 (d, 1H, *J* = 15.1 Hz), 7.57 (d, 2H, *J* = 8.0 Hz), 7.53–7.45 (m, 3H), 7.44 (d, 1H, *J* = 15.7 Hz), 7.03 (d, 2H, *J* = 8.3 Hz), 1.40 (s, 9H); ¹³C NMR spectrum (100 MHz, CDCl₃) in ppm: 190.7, 158.3, 144.7, 138.6, 132.7, 129.8, 129.6, 128.7, 128.59, 123.8, 120.8, 79.5, 29.0.

Trans-4-(4-methylphenoxy)chalcone (CH13): Yellow, resinous solid, 27 % yield. Soluble in chloroform, ethyl acetate, 1,4-dioxane. Insoluble in petroleum ether and water; ¹H NMR spectrum (400 MHz, CDCl₃) in ppm: 8.00 (d, 2H, *J* = 7.7 Hz), (d, 1H, *J* = 15.6 Hz), 7.60–7.30 (m, 5H), 7.43 (d, 1H, *J* = 15.6 Hz), 7.14 (d, 1H, *J* = 7.9 Hz), 6.94 (m, 4H), 2.32 (s, 3H); ¹³C NMR spectrum (100 MHz, CDCl₃) in ppm: 190.4, 160.3, 153.6, 144.2, 138.4, 133.9, 132.6, 132.5, 130.2, 128.6, 120.6, 119.8, 119.0, 118.1, 117.8, 20.7.

Trans-3-(4-methylphenoxy)chalcone (CH14): Yellow, resinous solid, 29 % yield. Soluble in chloroform, ethyl acetate, 1,4-dioxane. Insoluble in petroleum ether and water; ¹H NMR spectrum (400 MHz, DMSO-d₆) in ppm: 6.87 (d, 1H, *J* = 7.9 Hz), 6.65 (d, 1H, *J* = 15.1 Hz), 6.45–6.00 (m, 7H), 6.00 (d, 2H, *J* = 8.1 Hz), 5.80–5.75 (m, 3H), 5.48 (d, 1H, *J* = 15.1 Hz), 1.20 (s, 3H); ¹³C NMR spectrum (100 MHz, CDCl₃) in ppm: 189.3, 159.7, 153.2, 143.6, 133.7, 133.6,

131.0, 130.9, 130.7, 130.5, 128.9, 128.8, 128.6, 120.8, 119.7, 119.3, 117.8, 20.5.

(E)-1-phenyl-3-(thiophen-2-yl)prop-2-en-1-one (CH15): Beige solid, 29 % yield. Soluble in chloroform, ethyl acetate, 1,4-dioxane. Insoluble in petroleum ether and water; ¹H NMR spectrum (400 MHz, CDCl₃) in ppm: 8.01 (d, 2H, *J* = 8.1 Hz), 7.95 (d, 1H, *J* = 15.4 Hz), 7.48–7.52 (m, 3H), 7.41 (m, 1H), 7.35 (m, 1H), 7.33 (d, 1H, *J* = 15.4 Hz), 7.10–7.05 (m, 1H); ¹³C NMR spectrum (100 MHz, CDCl₃) in ppm: 190.0, 140.4, 138.2, 137.3, 132.9, 132.8, 132.2, 129.0, 128.7, 128.6, 128.5, 128.4, 120.8.

(E)-1-phenyl-3-(thiophen-3-yl)prop-2-en-1-one (CH16): Beige solid, 29 % yield. Soluble in chloroform, ethyl acetate, 1,4-dioxane. Insoluble in petroleum ether and water; ¹H NMR spectrum (400 MHz, CDCl₃) in ppm: 8.00 (d, 2H, *J* = 8.0 Hz), 7.81 (d, 1H, *J* = 15.6 Hz), 7.61–7.55 (m, 2H), 7.50 (t, 2H, *J* = 7.6 Hz), 7.43 (d, 1H, *J* = 5.5 Hz), 7.38–7.33 (m, 1H), 7.35 (d, 1H, *J* = 15.8 Hz); ¹³C NMR spectrum (100 MHz, CDCl₃) in ppm: 190.9, 138.4, 138.3, 138.2, 132.9, 129.4, 129.3, 128.8, 128.7, 128.6, 127.2, 125.3, 121.9.

* For Comparison between ³*J*_{trans H[−]H}/Hz experimental and calculated. See Table 1.

2.3. Coating preparation

Commercially available carbon steel (CS) was used as feedstocks. To carry out the tests (weight loss experiments, electrochemical measurements, and surface study), the sample of CS was mechanically rubbed with emery paper up to 1200 to obtain a homogeneous surface. The coatings on the CS with chalcone were carried out by drying at 40 °C the 1.0x10^{−3} M chalcone solution within which there was the CS. Before being used in all the experiments, CS-chalcone was washed with deionized water.

2.4. Weight loss experiments

The steel specimens had a cylinder form with the following dimensions: 0.3 cm (diameter) × 1.0 cm (height). The weight

Table 1 Yield for the synthesis of chalcones CH1-16 employing methods A and B. Comparison between ³*J*_{trans H[−]H}/Hz experimental and calculated.

Product	R ¹	Yield / %		Experimental ³ <i>J</i> _{transH-H} /Hz	Calculated ³ <i>J</i> _{transH-H} /Hz	%error
		Method A	Method B			
CH1	Ph	75	72	15.7	15.7	0.00 %
CH2	4-Cl-Ph	83	35	15.7	15.7	0.00 %
CH3	4-Me ₂ N-Ph	34	36	15.5	15.6	0.64 %
CH4	4-OH-Ph	27	33	15.5	15.6	0.64 %
CH5	4-NH ₂ -Ph	35	37	15.2	15.6	2.56 %
CH6	2-NH ₂ -Ph	33	36	11.7	15.7	25.48 %
CH7	4-NO ₂ -Ph	75	12	15.5	15.7	1.27 %
CH8	4-MeO-Ph	38	35	15.6	15.6	0.00 %
CH9	4-Br-Ph	69	33	15.7	15.6	0.64 %
CH10	4-BnO-Ph	41	39	15.6	15.6	0.00 %
CH11	4-Ph ₂ N-Ph	32	31	15.6	15.6	0.00 %
CH12	4-BuO-Ph	31	33	15.7	15.7	0.00 %
CH13	4-(4-MePhO)-Ph	27	28	15.3	15.6	1.92 %
CH14	3-(4-MePhO)-Ph	29	27	15.1	15.6	3.21 %
CH15	2-Th	83	22	15.4	15.5	0.65 %
CH16	3-Th	85	17	15.6	15.5	0.65 %

loss test was performed to depict the actual corrosion in the natural state using a precision balance. Following the soaking process for 1 week in 1.0 M HCl solution, the CS samples were taken out, dried, and weighed accurately again. The experiments were repeated three times for each group of samples. The average weight loss was reported to calculate the corrosion rate values in centimeters per hour (cm h^{-1}), which was determined using the reference reported by (Scully and Babouian, 1995).

2.5. Electrochemical measurements

The potentiodynamic polarization (PDP) and the impedance spectroscopy (EIS) were carried out in a conventional three-electrode cell to investigate the electrochemical behavior of CS - Chalcone coating in 1.0 M HCl solutions. It was used as a platinum counter electrode and a saturated Ag/AgCl electrode as the reference electrode. The working electrode of cylinder shape has a dimension of 0.070 cm^2 and is in contact with the electrolyte. These experiments were performed by Origaflex electrochemical working station (OGF500 potentiostat/galvanostat with impedance, France) and "OrigaMaster 5" software. The CS - Chalcone was immersed into the solution (100 mL in volume) at the temperature of 30°C , and the open circuit potential was obtained before making the EIS and PDP methods. The PDP experiment was programmed to take place from -1200 mV to 0.0 mV for the corrosion potential with a scan rate of 1 mV s^{-1} . The EIS measurements were carried out by the amplitude of 5 mV and varying the frequency from 1 Hz to 100 kHz . All results were performed at least three times looking for reproducibility (Fouda, 2014).

2.6. Surface study

The characterization of surface for Scanning electron microscopy (SEM) was used to know the morphology of the carbon steel after immersed in acid medium with two chalcones (CH15 and CH16) on surface and without chalcone at 20°C . Thereafter, the samples were removed, rinsed with deionized water, and finally analyzed by SEM using QUANTA 200 FEI.

3. Results and discussion

3.1. Synthesis

Two different methodologies were evaluated to synthesize the compounds CH1-16: reactions at room temperature (method A) and solvent-free microwave-assisted reactions (method B) (Nama et al, 2016).

The standard Claisen-Schmidt methodology used in methods A and B involves a crossed-condensation reaction between acetophenone and an aldehyde in a basic medium. A series of aldehydes with different substituents were used to optimize the reaction conditions and evaluate the effect of the starting aldehyde's electronic character. Benzaldehyde was used as an initial study model, carrying out the reaction at 0°C in ethanol, in the exact stoichiometric quantities as acetophenone and potassium hydroxide, the latter used as a base. It was evident that the reaction proceeded at that temperature only after 8 h. However, the number of equivalents was diminished to

evaluate the base's catalytic effect. It was evidenced that using 1/10 of equivalents concerning acetophenone (10 % mol), the reaction was cleaner, according to the chromatographic profiles obtained using TLC (silica gel as stationary phase and a mixture of ethyl acetate: hexane 2:8 as mobile phase). Once the base concentration was established, we wanted to evaluate the optimum temperature. For this, tests were carried out at 0, 5, 10, and 18°C (room temperature) for 8 h. The results showed that the percent yield increased as the reaction temperature increased (Table 1). An essay on reflux conditions was carried out; however, TLC's chromatographic profile showed the formation of multiple products, which suggests the favoring of side reactions. Once the reaction conditions were established for the benzaldehyde-acetophenone model, other p-substituted aldehydes were used. The results showed that aldehydes with electron-withdrawing groups react more efficiently and with better yields (Table 1) than those with electron-donor groups, which is an expected result since electron-poor aldehydes tend to have a higher electrophilic character.

Method B's reaction conditions were optimized to improve the yield percentage for obtaining chalcones derived from aldehydes with electron-donor groups. A benzaldehyde-acetophenone model was used using potassium hydroxide at 10 % mol in the absence of solvent and microwave irradiation of 10 W without exceeding 18°C , trying to evaluate the non-thermal effect of microwave irradiation. However, it was evidenced that the reaction did not proceed under these conditions, so the microwave reactor's power was increased while maintaining a constant temperature. Thus, the following temperatures were evaluated: 40, 60, 80, and 120°C . Reactions were monitored by TLC using the afore mentioned chromatographic system. The profiles obtained showed that the reaction started at 80°C in the absence of solvent. However, it required an irradiation time of at least one hour to ensure the consumption of the reagents. Furthermore, it was evidenced that long reaction times under these conditions increased the number of side reactions.

For this reason, it was decided to evaluate a temperature of 120°C at different reaction times. As a result, it was found that the starting reagents were consumed entirely within 10 min of irradiation, keeping the mentioned temperature constant. These conditions were used for the other aldehydes evaluated; however, it was evidenced that the performance of chalcones derived from aldehydes with electron-withdrawing groups was significantly reduced, and the number of by-products increased. On the other hand, a slight increase in the yield percentage was evidenced for chalcones derived from aldehydes with electron-donor groups, which was not very significant (Table 1). For this reason, it was decided to use method A as a strategy to obtain the CH1-16 compounds for subsequent tests.

3.2. Weight loss measurements

This study was essential to select that non-soluble chalcone would be used as a carbon steel corrosion inhibitor and be analyzed with PDP and EIS techniques. The corrosion rate (v), inhibitory efficiency (η) values without and with, and the degree of surface coverage (θ) are identified in Table 2. The calculated corrosion rate values in centimeters per hour (cm h^{-1}), the protection abilities (η), and degree of surface coverage (θ)

Table 2 Weight loss parameters of the CS immersed in the solution without and with a different mass of the non-soluble chalcones at 20° C.

Inhibitors	Mass (mg)	Weight loss (g)	v (cm/h)	η_{WL} (%)	θ
Blank		0.0534	1.3625	—	—
CH4	0.5	0.0503	1.2834	5.80	0.06
CH9	0.6	0.0537	1.3702	—	—
CH10	1.5	0.0538	1,3727	—	—
CH11	2.8	0.0499	1.2732	6.55	0.06
CH15	2.8	0.0400	1.0206	25.09	0.25
CH16	4.3	0.0480	1.2247	10.11	0.10

were using the following Eq (1), Eq. (2), and Eq. (3) (Chaouiki, 2020). We can see that the values of inhibitory efficiency to the CH9 and CH10 chalcones do not have a prominent role in corrosion inhibition. Conversely, the chalcones with CH4, CH11, CH15, and CH16 moieties prevented the corrosion of the metallic surface, which can be seen in the inhibitory efficiency values of 6.55, 5.80, 25.09, and 10.11 %, respectively. Notably, the CH15 has the highest inhibitory effect on the other chalcones. This might be explained by the fact that absorption of the compound on the surface was maximal for the interaction with unshared electron pairs on the Sulphur (Assad, 2021) and the position of the thiophene group in chalcone.

$$v = \frac{K \times W}{A \times t \times \rho} \quad (1)$$

$$\eta_{wL}(\%) = \frac{v_o - v}{v} \times 100\% \quad (2)$$

$$\theta = \frac{v_o - v}{v} \quad (3)$$

3.3. Data using potentiodynamic measurements

The behaviors of the non-soluble chalcones were tested by the potentiodynamic polarization technique to acquire more information. Still, only three out of the four chalcones showed polarization curves with apparent corrosion inhibition. Therefore, the cathodic and anodic polarization plots of CS in 1.0 M HCl solutions without and with various amounts of masses deposited are represented in Fig. 1. In addition, the values associated with electrochemical parameters such as corrosion electrode potential E_{corr} (mV), anodic and cathodic slopes β_a and β_c (mV/dec), corrosion current density i_{corr} ($\mu\text{A cm}^{-2}$) as well as inhibition efficiencies η_{PDP} (%) are given in Table #3. The values of inhibition efficiency were estimated using Eq. (4).

$$E_{PDP}(\%) = \left[1 - \frac{i_{corr}}{i_{corr}^0} \right] \times 100 \quad (4)$$

Where i_{corr} and i_{corr}^0 are the corresponding current densities of the Carbon Steel sample with and without the addition of the chalcones, respectively. Fig. 1 shows that the cathodic branch for all chalcones are quasi-parallel lines and very close to the blank curves, suggesting that the coating with non-soluble chalcones does not change the mechanism of hydrogen evolution. On the other hand, the CH15 has a significant change in the shape of the anodic branch (Fig. 1a) than the

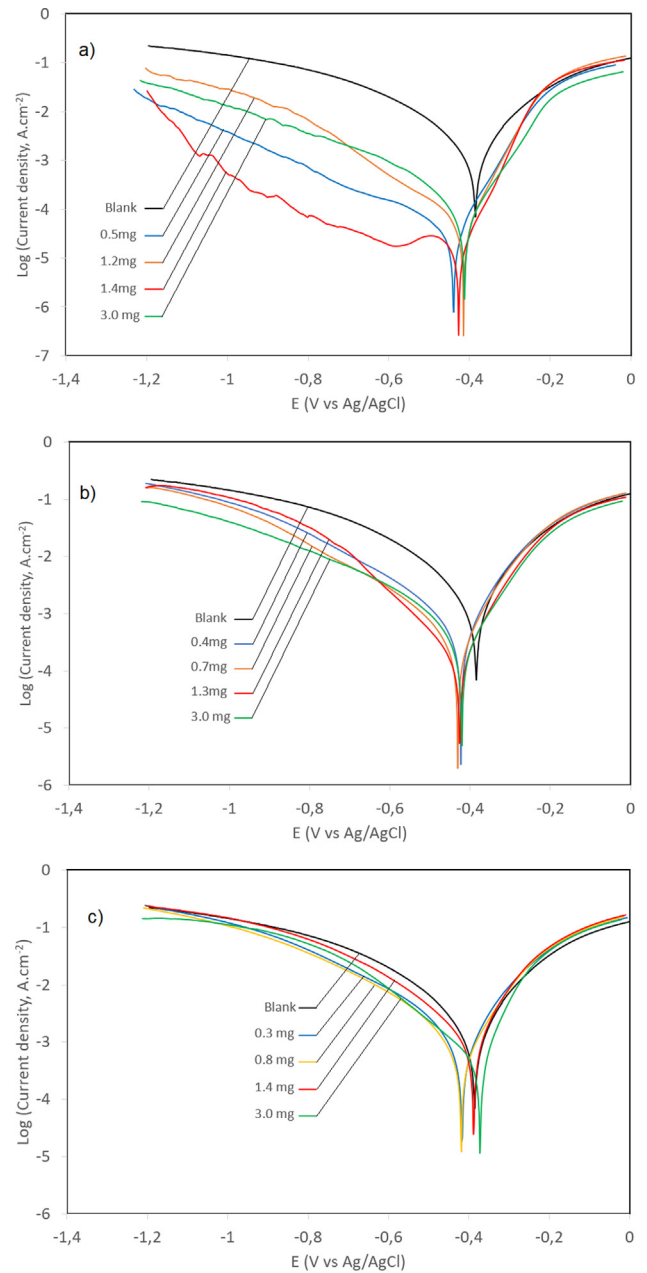


Fig. 1 Tafel curves of carbon steel electrode in 1.0 M HCl in the absence and presence of non-soluble chalcone at 20 °C.

other chalcones. This suggests some possible change in the mechanism of anodic dissolution reactions. Besides, note that the corrosion current densities (i_{corr}) decrease as the amount increases of deposited chalcones on the surface of Carbon Steel. The CH15 and CH16 showed maximum inhibition of approximately 1.4 mg.

In comparison, the CH11 showed maximum inhibition of 3.0 mg (Table 3), implying a maximum surface saturation point for corrosion inhibition as occurs with maximum inhibition concentrations for soluble chalcones (Lgaz, 2017; Chaouiki, 2020). These results are further confirmed in E_{corr} displacement at values more negative and less than 85 mV, suggesting that non-soluble chalcones behave as mixed-type inhibitors. Finally, the non-soluble chalcone efficiencies are tabulated in Table 3 where it was concluded that the presence

Table 3 Potentiodynamic polarization results for CS samples in 1.0 M HCl without and with non-soluble chalcones at 20 °C.

Inhibitors	Mass(mg)	-E _{corr} (mV vs Ag/AgCl)	-β _c (mV dec ⁻¹)	β _a (mV dec ⁻¹)	I _{corr} (mA.cm ⁻²)	η _{PDP} (%)	θ
Blank	–	389.9	173.3	124.1	1.4718	–	–
CH11	0.3	416.8	293.3	164.0	2.059	–	–
	0.8	418.8	258.8	144.6	1.4982	–	–
	1.4	387.9	169.5	92.0	0.9383	36	0.36
	3.0	371.2	176.3	68.3	0.4437	70	0.70
CH15	0.5	439.6	491.5	88.4	0.0714	95	0.95
	1.2	415.2	172.4	67.5	0.0425	97	0.97
	1.4	424.2	571.1	66.9	0.0134	99	0.99
	3.0	411.8	171.9	92.5	0.0289	98	0.98
CH16	0.4	422.8	256.3	129.5	0.8483	42	0.42
	0.7	429.6	207.2	109.9	0.4145	72	0.72
	1.4	424.0	155.8	90.4	0.1814	88	0.88
	3.0	420.4	255.8	133.0	0.5955	60	0.60

of two thiophene groups in the chalcone raises their protective property. In contrast, other groups such as CH11 were less efficient.

3.4. Data using electrochemical impedance spectroscopy

Nyquist diagrams of non-soluble chalcones on the carbon steel are shown in Fig. 2 and enable us to distinguish better the corrosion behavior and the elementary phenomena involved in the metal/solution interface. As illustrated in Fig. 2, the carbon steel without and with chalcones, for all amounts, reveals a single semicircle adequately centered on the axis of the impedance real part. The Nyquist diagrams are not perfect semicircles and may be due to the roughness and inhomogeneous electrode surface. But the shapes of the Nyquist diagrams exhibit the dissolution of carbon steel in hydrochloric acid is principally regulated by the charge transfer, meaning that the mechanism does not change when the three non-soluble chalcones are adsorbed. The mechanism does not change when the three non-soluble chalcones are adsorbed. Additionally, these semicircles increase with increasing non-soluble chalcone amounts, i.e., the absorption of these molecules on the carbon steel surface suggests the formation of a stable, protective film.

The equivalent circuit used to study the EIS spectra can be fitted in Fig. 3 and Table 4. First, a list of the values of EIS parameters, including the inhibition efficiency, were calculated by Eq. (5), where R_P° and R_P are charge transfer resistances without and with tested non-soluble chalcones, respectively. Next, the interfacial capacitance C_{dl} was calculated from CPE parameter values Q and n using the Eq. (6), where Q is the magnitude and n is the exponential term of a CPE that can be used to measure surface inhomogeneity.

$$\eta_{EIS}(\%) = \left[\frac{R_P - R_P^\circ}{R_P} \right] \times 100 \quad (5)$$

$$C_{dl} = \sqrt[n]{Q \times R_P^{1-n}} \quad (6)$$

Table 4 shows that the values of the parameter R_p increase on increasing the inhibitor amounts. These results indicate that the corrosion rate decreases in conformity with type chalcone: CH11 (57 %) < CH16 (85 %) < CH15 (89 %). This order is according to that obtained from Potentiodynamic Polarization measurements. Therefore, according to these results, we can

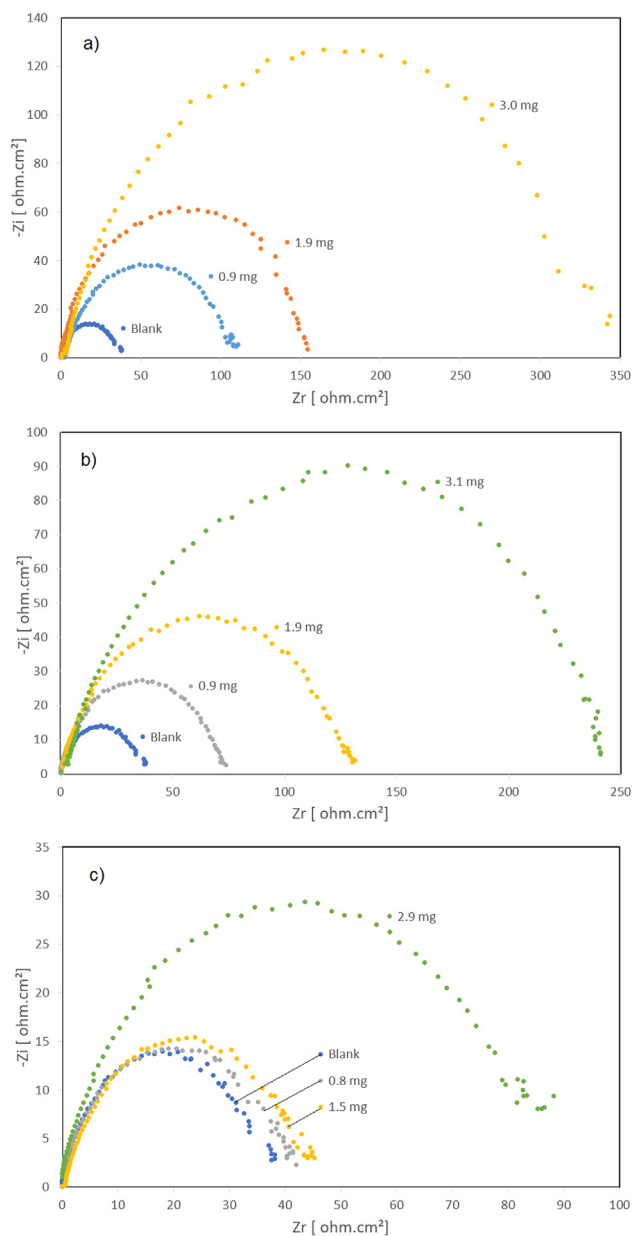


Fig. 2 EIS curves of carbon steel electrode in 1.0 M HCl in the absence and presence of non-soluble chalcone at 20 °C.

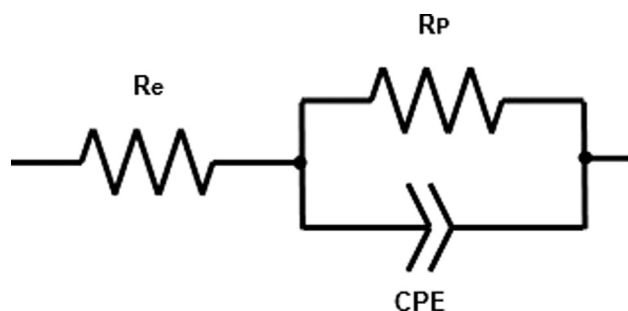


Fig. 3 The electrochemical equivalent circuit used to fit the impedance spectra.

infer that the unshared electron pairs on the Sulphur (Assad, 2021), are adsorbed on the Carbon Steel surface for retarding the corrosion.

3.5. Surface characterization by SEM

The characterization of surface topography for carbon steel by SEM has provided visual information on how the chalcone significantly inhibited corrosion. As shown in Fig. 4, the carbon steel electrode after exposure to 1.0 M HCl solution without inhibitor (Fig. 4.a) is hugely rough and grainy. Opposite to

this, the surface of the carbon steel with CH15 (Fig. 4.b) and with CH16 (Fig. 4.c) are smoother due to the inhibitory effect and that also observed in PDP and EIS. Although, the surfaces with inhibitors are not exempt totally from corrosion since there are areas with gray and white zones, which correspond to the dandruff of iron oxide, and that is due to the inhomogeneity of the coating. In Fig. 5, can be observed that the surface steel with CH15 was strongly protected from oxidizing agent. Conversely, on carbon steel with CH16 there are cracks and white areas due to increased surface oxidation, although to a lesser degree than uncoated steel.

3.6. Density functional Theory calculations

In order to explain the measured corrosion decrease assisted by compounds CH11, CH15, and CH16, computational calculations were performed using the DFT B3YLP methodology at the level 6-311G* (Becke, 1993, 1988). Table 5 presents the calculated values for several quantum descriptors such as total energy, dipolar moment, and the frontier molecular orbital energies for HOMO and LUMO. These descriptors can be used to establish the molecular features determining the decreasing corrosion phenomena (Cherrad et al., 2022). In this sense, the total energy value established a correlation between our results and the chalcone chemical stability in different reaction conditions, including oxidative-reductive reactions.

Table 4 Electrochemical impedance spectroscopy results for CS samples in 1.0 M HCl without and with non-soluble chalcones at 20 °C.

Inhibitors	Mass(mg)	$R_p (\Omega \times \text{cm}^2)$	n	$Q \times 10^{-4} (\text{S}^n \Omega^{-1} \text{cm}^{-2})$	$C_{dl} (\mu\text{F}/\text{cm}^2)$	$\eta_{\text{EIS}} (\%)$	θ
Blank	–	36.54	0.78	4.4803	137.73	–	–
CH11	0.8	41.88	0.73	5.0460	120.13	12.75	0.13
	1.5	43.29	0.80	4.1174	146.31	15.59	0.16
	2.9	86.24	0.75	2.5918	73.45	57.63	0.58
CH15	0.9	104.84	0.80	1.3623	48.01	65.15	0.65
	1.9	159.25	0.82	0.7612	28.16	77.05	0.77
	3.0	334.06	0.82	0.3969	15.06	89.06	0.89
CH16	0.9	72.11	0.79	2.3719	78.30	49.33	0.49
	1.9	127.54	0.78	1.1575	35.17	71.35	0.71
	3.1	243.95	0.82	0.5338	20.64	85.02	0.85

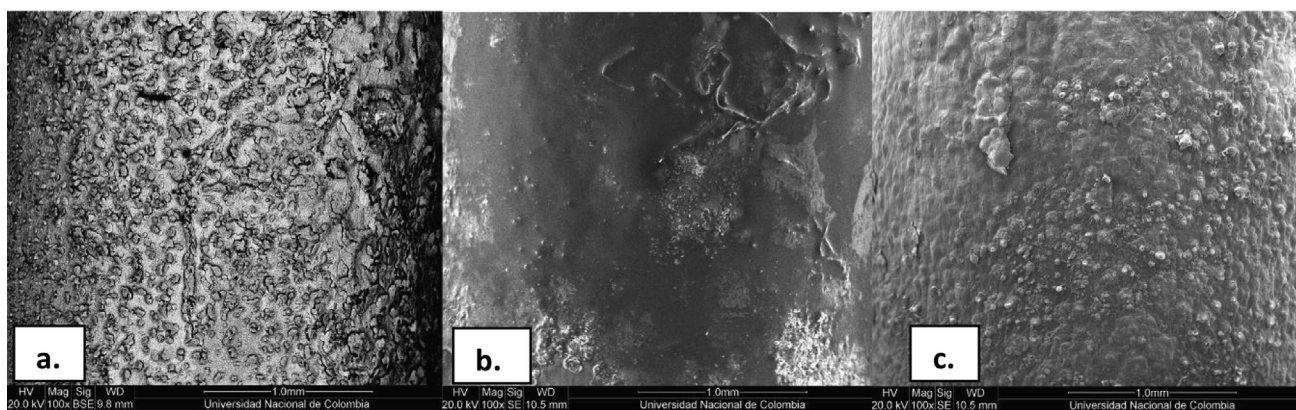


Fig. 4 SEM micrographs at 1.0 mm of carbon steel surface (a) without inhibitor, (b) with CH15 and (c) with CH16 after 30 min of immersion in 1.0 M HCl. The mass of chalcone on steel was of 2.9 mg.

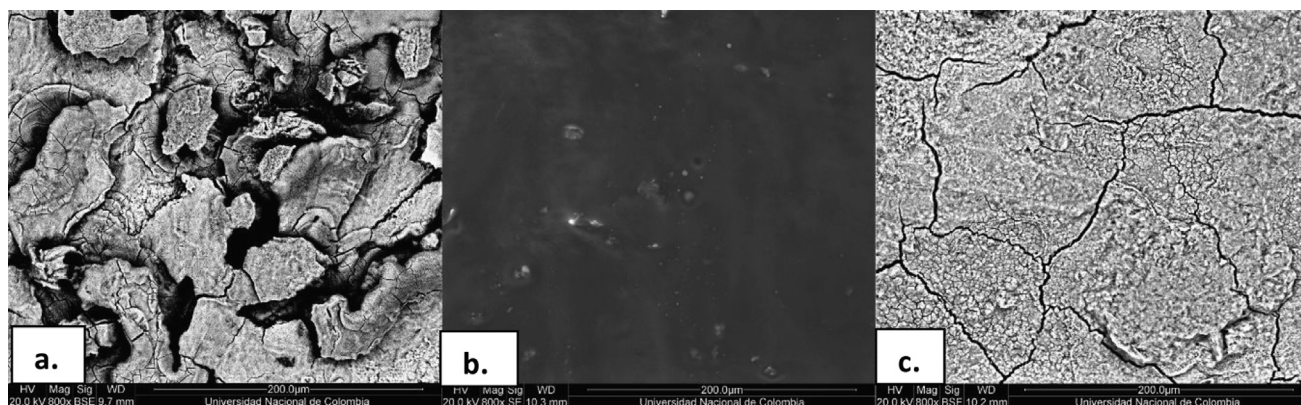


Fig. 5 SEM micrographs at 200 μm of carbon steel surface (a) without inhibitor, (b) with CH15 and (c) with CH16 after 30 min of immersion in 1.0 M HCl. The mass of chalcone on steel was of 2.9 mg.

Table 5 Calculated quantum descriptors for compounds CH1-CH16.

Product	R ¹	E/ au	HOMO/ eV	LUMO/ eV	Dipolar moment/ D	Gap HOMO-LUMO/ eV
CH1	Ph	-654.1	-6.64	-2.03	3.65	4.61
CH2	4-Cl-Ph	-1113.7	-6.71	-2.21	3.91	4.50
CH3	4-Me ₂ N-Ph	-788.1	-5.68	-1.79	5.41	3.89
CH4	4-OH-Ph	-729.4	-6.17	-1.87	3.48	4.30
CH5	4-NH ₂ -Ph	-709.5	-5.76	-1.72	5.87	4.04
CH6	2-NH ₂ -Ph	-709.5	-5.97	-1.86	4.52	4.11
CH7	4-NO ₂ -Ph	-858.7	-7.13	-2.91	4.41	4.22
CH8	4-MeO-Ph	-768.7	-6.08	-1.84	4.09	4.24
CH9	4-Br-Ph	-3227.7	-6.66	-2.22	3.92	4.44
CH10	4-BnO-Ph	-999.8	-6.14	-1.90	3.44	4.24
CH11	4-Ph ₂ N-Ph	-1171.7	-5.41	-1.89	4.85	3.52
CH12	4-BuO-Ph	-886.7	-6.37	-1.95	3.73	4.42
CH13	4-(4-MePhO)Ph	-999.8	-6.1	-1.86	4.31	4.24
CH14	3-(4-MePhO)Ph	-999.8	-6.32	-1.99	4.31	4.33
CH15	2-Th	-974.9	-6.55	-1.92	3.19	4.63
CH16	3-Th	-974.9	-6.44	-2.06	3.20	4.38

Thus, CH9 and CH11 showed the lowest total energy values, indicating they are the most stable compounds of the series. On the other hand, CH1 and CH6 presented the highest total energy values suggesting they are the most unstable compounds. We explain these results considering the functional groups for each compound: the aromatic conjugated pi system in CH11 is affected by the presence of electron donor groups attached in the 4-position (R = Ph₂NH), whose electronic consequence is the increase of the electron-density by a “mesomeric” or resonance effect through the high extended π -system (Fig. 6a) (Prabhu et al., 2013). Although compound CH6 counts with a primary amine group attached to the 2-position, presumably, this “mesomeric” or resonance effect could be minor in comparison with compound CH11 by the absence of additional aromatic rings attached to the amine group. For compound CH9, a heavy atom such as bromine as a substituent tends to reduce the total energy value. Bromine substituent could improve the electron density of the extended π -system by a short mesomeric effect leading to a low total energy value (Balci, 2005). The dipole moment is associated with the tendency of the chalcones to dissolve in a polar medium (Saidman et al., 2002), such as the one used in

the electrochemical experiments. It is known that chalcones can undergo Michael reactions when they meet different nucleophiles in the reaction medium (Al-Jaber et al., 2012), forming a bond between the nucleophile and carbon 3 concerning the carbonyl (Scheme 2). The medium used for corrosion inhibition measurement experiments may contain nucleophilic species such as water or hydroxyl ions from moisture in the medium. In this sense, a high dipole moment would suggest a greater tendency for the chalcone to dissolve in the medium and subsequently undergo the different degradation pathways through an initial Michael reaction (Danilov, 1960; Hashemi et al., 2006; Van Dyke and Pritchard, 1967). The CH3 and CH5 compounds showed the highest values for dipole moment.

The calculated Fukui index (Sánchez-Márquez, 2019), confirmed that the labeled C7, C8, and C9 atoms in the propen-1-one fragment showed the highest electrophilicity (Fig. 6b). These results can be correlated with their null behavior as corrosion inhibitors. The compounds CH15 and CH16 presented the lowest values for the dipole moment, suggesting that they have the lowest solubility in the polar medium used and, therefore, the lowest tendency to degrade. These results correlate

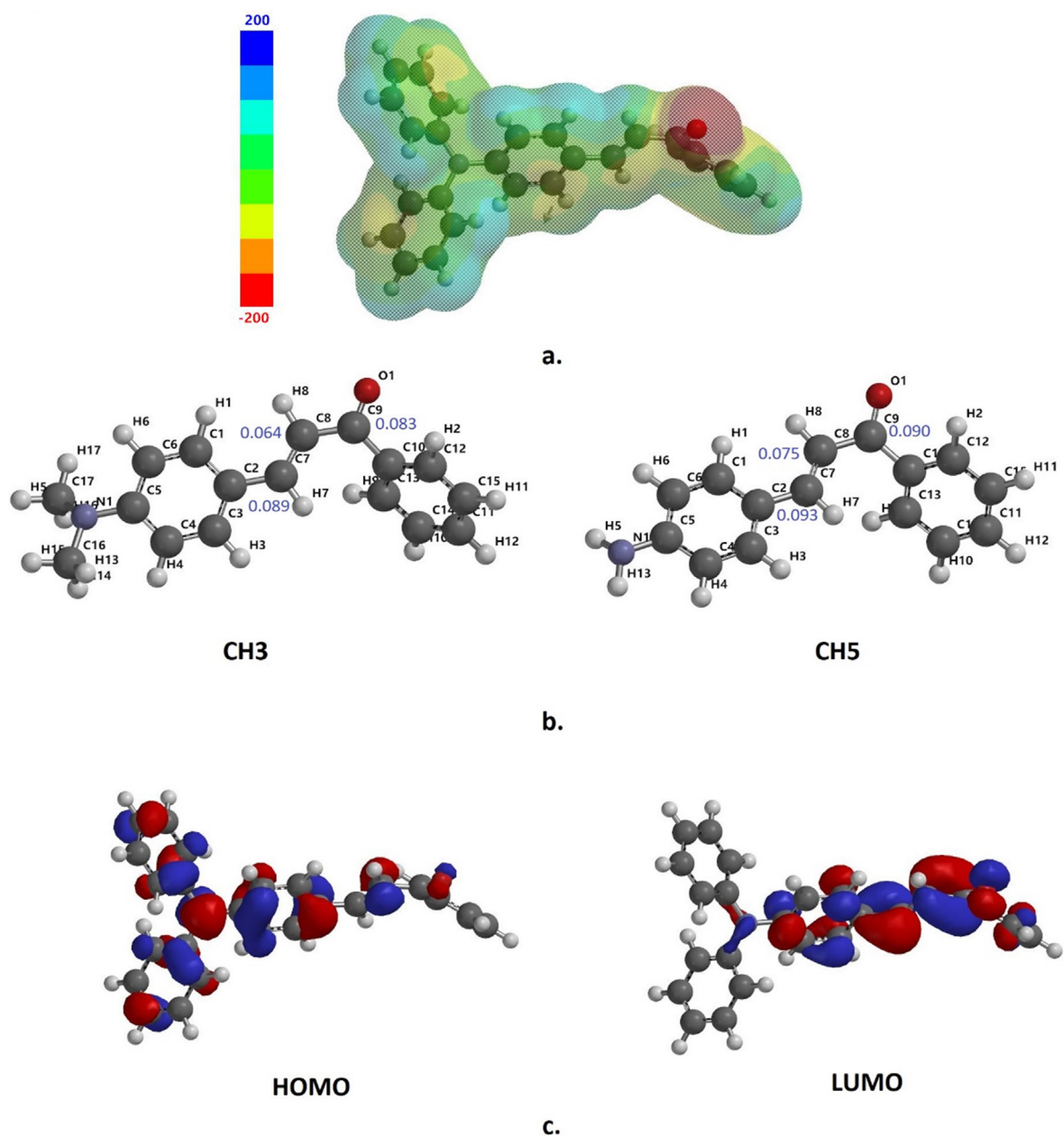


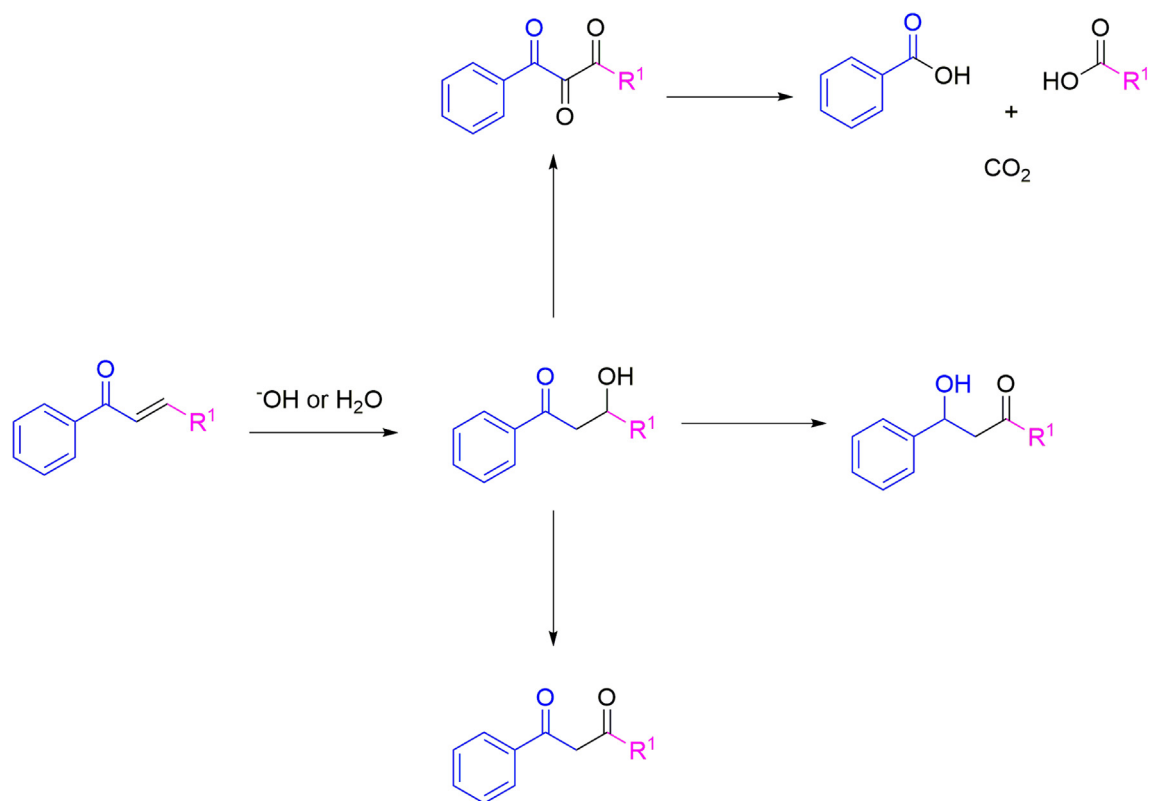
Fig. 6 A) Electrostatic potential map of compound CH11 (isovalue: 0.002); b) calculated fukui index for electrophilicity in compounds CH3 and CH5; c) HOMO and LUMO tridimensional representations of compound CH11.

with the results obtained, especially for compounds CH15 and CH16, showing that the corrosion inhibition capacity is directly related to the low solubility of the coating used and that it is necessarily a process that occurs superficially as has been demonstrated in our experiments. Frontier molecular orbitals also correspond to excellent quantum descriptors that can be used to understand our results. It is known that a molecule can have more ability to donate electrons if the energy of the highest HOMO is high, while its ability to accept electrons is associated with a low value of LUMO (Cherrad et al., 2022). In this sense, CH11 has strong electron-donating power, followed by the CH3 and CH5 compounds. However, in the case of electron-accepting power, compound CH7 shows the highest electron-accepting characteristic, followed by CH9 and

CH2. The energy gap HOMO-LUMO, which can also be used as a descriptor, indicates the stability of a molecule: a high gap is considered high stability, and a low gap is associated with high reactivity.

4. Conclusion

The synthesis of the chalcones CH2, CH7, CH9, CH15, and CH16 was done at room temperature, and their performance percentages were considerably better than the microwave irradiation method. Furthermore, the methodology used in corrosion inhibition assays is standardized and can be applied to different types of molecules with various substituents. Finally, the chalcones CH11, CH15, and CH16 decreased corrosion in the PDP and EIS analyses. The HOMO-LUMO gap



Scheme 2 Proposed degradation pathways for high soluble chalcones.

results show that compound CH11 has the lowest energy gap, followed by compounds CH3 and CH5 (Fig. 6c), which suggests that CH11 has the highest reactivity in the group of molecules evaluated and that explains its ability to corrosion inhibition.

Declaration of Competing Interest

The authors declare that they have no known competing financial interests or personal relationships that could have appeared to influence the work reported in this paper.

Acknowledgments

The present work is a product derived from the project INV-CIAS-3134 funded by Vicerrectoría de Investigaciones at UMNG–Validity 2020-21.

References

- Abegão, L.M.G., Santos, F.A., Fonseca, R.D., Barreiros, A.L.B.S., Barreiros, M.L., Alves, P.B., Costa, E. V., Souza, G.B., Alencar, M.A.R.C., Mendonça, C.R., Kamada, K., De Boni, L., Rodrigues, J.J., 2020. Chalcone-based molecules: Experimental and theoretical studies on the two-photon absorption and molecular first hyperpolarizability. *Spectrochim. Acta Part A Mol. Biomol. Spectrosc.* 227, 117772. <https://doi.org/10.1016/j.saa.2019.117772>.
- Al-Jaber, N.A., Bougasim, A.S.A., Karah, M.M.S., 2012. Study of Michael addition on chalcones and or chalcone analogues. *J. Saudi Chem. Soc.* 16, 45–53. <https://doi.org/10.1016/J.JSCS.2010.10.017>.
- Assad, H., Kumar, A., 2021. Understanding functional group effect on corrosion inhibition efficiency of selected organic compounds. *J. Mol. Liq.* 344, 117755.
- Balci, M., 2005. Chemical Shift, in: *Basic 1H- and 13C-NMR Spectroscopy*. Elsevier, pp. 283–292. <https://doi.org/10.1016/B978-044451811-8.50012-7>.
- Becke, A.D., 1988. Density-functional exchange-energy approximation with correct asymptotic behavior. *Phys. Rev. A* 38, 3098–3100. <https://doi.org/10.1103/PhysRevA.38.3098>.
- Becke, A.D., 1993. Density-functional thermochemistry. III. The role of exact exchange. *J. Chem. Phys.* 98, 5648–5652. <https://doi.org/10.1063/1.464913>.
- Blasco, A.J., González, M.C., Escarpa, A., 2004. Electrochemical approach for discriminating and measuring predominant flavonoids and phenolic acids using differential pulse voltammetry: towards an electrochemical index of natural antioxidants. *Anal. Chim. Acta* 511, 71–81. <https://doi.org/10.1016/j.aca.2004.01.038>.
- Bouklah, M., Hammouti, B., Aouniti, A., Benkaddour, M., Bouyanzer, A., 2006. Synergistic effect of iodide ions on the corrosion inhibition of steel in 0.5M H₂SO₄ by new chalcone derivatives. *Appl. Surf. Sci.* 252, 6236–6242. <https://doi.org/10.1016/j.apsusc.2005.08.026>.
- Chaouiki, A., Lgaz, H., Salghi, R., Chafiq, M., Oudda, H., Shubhaxlaxmi, Bhat, K.S., Cretescu, I., Ali, I.H., Marzouki, R., Chung, I.-M., 2020. Assessing the impact of electron-donating-substituted chalcones on inhibition of mild steel corrosion in HCl solution: Experimental results and molecular-level insights. *Colloids Surfaces A Physicochem. Eng. Asp.* 588, 124366. <https://doi.org/10.1016/j.colsurfa.2019.124366>.
- Cherrad, S., Alrashdi, A.A., Lee, H.-S., El aoufir, Y., Lgaz, H., Satrani, B., Ghanmi, M., Aouane, E.M., Chaouch, A., 2022. Cupressus arizonica fruit essential oil: A novel green inhibitor for acid corrosion of carbon steel. *Arab. J. Chem.* 15, 103849. <https://doi.org/10.1016/j.arabjc.2022.103849>.
- Danilov, S.N., 1960. Mechanism of intramolecular oxidation-reduction reactions of β -hydroxy and β -halo carbonyl compounds. *Bull. Acad. Sci. USSR Div. Chem. Sci.* 9, 1964–1970. <https://doi.org/10.1007/BF00912046>.

- Doménech-Carbó, A., da Silveira, G.D., Medina-Alcaide, M.Á., Carmona, A.M., López-Serrano, D., Pasies-Oviedo, T., Algarra-Pardo, V.M., de Carvalho, L.M., Montoya, N., 2018. Polythiophenes as markers of asphalt and archaeological tar pitch aging. Characterization using solid-state electrochemistry. *Electrochem. Commun.* 87, 18–21. <https://doi.org/10.1016/j.elecom.2017.12.020>.
- A.S. Fouda, K. Shalabi, G.Y. Elewady, H.F.M., 2014. Chalcone Derivatives as Corrosion Inhibitors for Carbon Steel in 1 M HCl Solutions. *Int. J. Electrochem. Sci.* 9, 7038–7058.x|.
- A.S. Fouda, A.F. Hassan, M.A. Elmorsi, T.A. Fayed, A.A., 2014. Chalcones as Environmentally-Friendly Corrosion Inhibitors for Stainless Steel Type 304 in 1 M HCl Solutions. *Int. J. Electrochem. Sci.* 9, 1298–1320.
- Fouda, A.S., Gadow, H.S., El-Shafei, A.A., 2003. Chalcones as corrosion inhibitors for nickel in HCl and H₂SO₄ solutions. *Korroz. Figy.* 43, 95.
- Hashemi, M.M., Naeimi, H., Shirazizadeh, F., Karimi-Jaberi, Z., 2006. Oxidation of α -hydroxy ketones to diketones by iodic acid supported on alumina. *J. Chem. Res.* 2006, 345. <https://doi.org/10.3184/030823406777946653>.
- Katharotiya, P.D.S., 2021. Synthesis, characterization and investigation of chalcone as corrosion inhibitors for mild steel in hydrochloric acid. *Eur. Chem. Bull.* 10, 199–204.
- Kumar, B., Vashisht, H., Goyal, M., Kumar, A., Benhiba, F., Prasad, A.K., Kumar, S., Bahadur, I., Zarrouk, A., 2020. Study of adsorption mechanism of chalcone derivatives on mild steel-sulfuric acid interface. *J. Mol. Liq.* 318, <https://doi.org/10.1016/j.molliq.2020.113890> 113890.
- Lgaz, H., Subrahmanya Bhat, K., Salghi, R., Shubhalaxmi, Jodeh, S., Algarra, M., Hammouti, B., Ali, I.H., Essamri, A., 2017. Insights into corrosion inhibition behavior of three chalcone derivatives for mild steel in hydrochloric acid solution. *J. Mol. Liq.* 238, 71–83. <https://doi.org/10.1016/j.molliq.2017.04.124>.
- Martínez-Cifuentes, M., Salazar, R., Escobar, C.A., Weiss-López, B. E., Santos, L.S., Araya-Maturana, R., 2015. Correlating experimental electrochemistry and theoretical calculations in 2'-hydroxy chalcones: the role of the intramolecular hydrogen bond. *RSC Adv.* 5, 50929–50937. <https://doi.org/10.1039/C5RA10140A>.
- Messaoudi, I., Aribi, I., Zaaboub, Z., Ayachi, S., Othman, M., Said, A.H., 2021. Electrosynthesis and characterization of a new semi-conducting oligomer deriving from a disubstituted chalcone: 4-dimethylamino-4'-methoxychalcone. *J. Mol. Struct.* 1231, <https://doi.org/10.1016/j.molstruc.2020.129810> 129810.
- Mishra, S., Tirkey, V., Ghosh, A., Dash, H.R., Das, S., Shukla, M., Saha, S., Mobin, S.M., Chatterjee, S., 2015. Ferrocenyl-cymantrenyl hetero-bimetallic chalcones: Synthesis, structure and biological properties. *J. Mol. Struct.* 1085, 162–172. <https://doi.org/10.1016/j.molstruc.2014.12.070>.
- N. Nama, N. Mameda, S. Peraka, S. Kodumuri, D. Chevella, R. Banothu and V. Amrutham, *RSC Adv.*, 2016. Synthesis of α,β -Unsaturated Ketones from Alkynes and Aldehydes over H β Zeolite under Solvent-Free Conditions. DOI: 10.1039/C6RA11593DRam-murthya,b Amrutham Vasub and Nama Narendera.
- I.B. Obot, E.E. Ebenso, Z.M.G., 2021. Eco-friendly Corrosion Inhibitors: Adsorption and Inhibitive Action of Ethanol Extracts of *Chromolaena Odorata* L. for the Corrosion of Mild Steel in H₂SO₄ Solutions. *Int. J. Electrochem. Sci.* 7, 1997–2008.
- Olasehinde, E.F., Agbaffa, B.E., Adebayo, M.A., Enis, J., 2022. Corrosion protection of mild steel in acidic medium by titanium-based nanocomposite of *Chromolaena odorata* leaf extract. *Mater. Chem. Phys.* 281, <https://doi.org/10.1016/j.matchemphys.2022.125856> 125856.
- Pérez-Cruz, F., Vazquez-Rodríguez, S., Matos, M.J., Herrera-Morales, A., Villamena, F.A., Das, A., Gopalakrishnan, B., Olea-Azar, C., Santana, L., Uriarte, E., 2013. Synthesis and Electrochemical and Biological Studies of Novel Coumarin-Chalcone Hybrid Compounds. *J. Med. Chem.* 56, 6136–6145. <https://doi.org/10.1021/jm400546y>.
- Pooja Singh, M.A., Quraishi, E.E., Ebenso, C.B.V., 2014. Ultrasound Assisted Synthesis of Chalcones as Green Corrosion Inhibitors for Mild Steel in 1M Hydrochloric Solution. *Int. J. Electrochem. Sci.* 9, 7446–7459.
- Prabhu, A.N., Upadhyaya, V., Jayarama, A., Subrahmanya Bhat, K., 2013. Synthesis, growth and characterization of π conjugated organic nonlinear optical chalcone derivative. *Mater. Chem. Phys.* 138, 179–185. <https://doi.org/10.1016/j.matchemphys.2012.11.041>.
- Ramagathan, B., Gopiraman, M., Olasunkanmi, L.O., Kabanda, M. M., Yesudass, S., Bahadur, I., Adekunle, A.S., Obot, I.B., Ebenso, E.E., 2015. Synthesized photo-cross-linking chalcones as novel corrosion inhibitors for mild steel in acidic medium: experimental, quantum chemical and Monte Carlo simulation studies. *RSC Adv.* 5, 76675–76688. <https://doi.org/10.1039/C5RA12097G>.
- K. Sahu, N., S. Balbhadra, S., Choudhary, J., V. Kohli, D., 2012. Exploring Pharmacological Significance of Chalcone Scaffold: A Review. *Curr. Med. Chem.* 19, 209–225. <https://doi.org/10.2174/092986712803414132>.
- Saidman, E., Yurquina, A., Rudyk, R., Molina, M.A.A., Ferretti, F. H., 2002. A theoretical and experimental study on the solubility, dissolution rate, structure and dipolar moment of flavone in ethanol. *J. Mol. Struct. THEOCHEM* 585, 1–13. [https://doi.org/10.1016/S0166-1280\(02\)00027-1](https://doi.org/10.1016/S0166-1280(02)00027-1).
- Sánchez-Márquez, J., 2019. Correlations between Fukui Indices and Reactivity Descriptors Based on Sanderson's Principle. *J. Phys. Chem. A* 123, 8571–8582. <https://doi.org/10.1021/acs.jpca.9b05571>.
- Scully, J., Baboian, R., 1995. *Standard Practice for Laboratory Immersion Corrosion Testing of Metals*, ASTM Phila. PA., 110
- Serifi, O., Tsopelas, F., Kypreou, A.-M., Ochsenschüh-Petropoulou, M., Kefalas, P., Detsi, A., 2013. Antioxidant behaviour of 2'-hydroxy-chalcones: a study of their electrochemical properties. *J. Phys. Org. Chem.* 26, 226–231. <https://doi.org/10.1002/poc.3071>.
- Shah, A., Qureshi, R., Khan, A.M., Khera, R.A., Ansari, F.L., 2010. Electrochemical behavior of 1-ferrocenyl-3-phenyl-2-propen-1-one on glassy carbon electrode and evaluation of its interaction parameters with DNA. *J. Venom. Anim. Toxins Incl. Trop. Dis.* 21. <https://doi.org/10.1590/S0103-50532010000300008>.
- Sharma, V.S., Sharma, A.S., Agarwal, N.K., Shah, P.A., Shrivastav, P.S., 2020. Self-assembled blue-light emitting materials for their liquid crystalline and OLED applications: from a simple molecular design to supramolecular materials. *Mol. Syst. Des. Eng.* 5, 1691–1705. <https://doi.org/10.1039/D0ME00117A>.
- Slobodinyuk, D.G., Shklyaeva, E.V., Abashev, G.G., 2020. Electrochemical oxidation of asymmetric chalcones containing two terminal electroactive moieties. *J. Appl. Electrochem.* 50, 757–766. <https://doi.org/10.1007/s10800-020-01434-z>.
- Tavares, E.M., Carvalho, A.M., Gonçalves, L.M., Valente, I.M., Moreira, M.M., Guido, L.F., Rodrigues, J.A., Doneux, T., Barros, A.A., 2013. Chemical sensing of chalcones by voltammetry: trans-Chalcone, cardamomin and xanthohumol. *Electrochim. Acta* 90, 440–444. <https://doi.org/10.1016/j.electacta.2012.12.040>.
- Van Dyke, M., Pritchard, N.D., 1967. Oxidation of α -hydroxy ketones with dimethyl sulfoxide. *J. Org. Chem.* 32, 3204–3205. <https://doi.org/10.1021/jo01285a064>.
- Velrani, S., Mahalakshmi, R., 2015. Investigation of inhibition effect of naphthyl chalcones on mild steel corrosion in sulphuric acid medium. *Rayasan J. Chem.* 8, 156–160.
- Yadav, G.D., Wagh, D.P., 2020. Claisen-Schmidt Condensation using Green Catalytic Processes: A Critical Review. *ChemistrySelect* 5, 9059–9085. <https://doi.org/10.1002/slct.202001737>.